Electronic Supplementary Material (ESI) for Nanoscale.

Chloride Enables the Growth of Ag Nanocubes and Nanowires by Making PVP Binding Facet-Selective

Heng Xu,†[a] Zihao Chen,†[b] Spencer Hao,[a] Kristen A. Fichthorn,*[b,c] and Benjamin J. Wiley*[a]

[a]Department of Chemistry, Duke University, Durham, NC 27708 (USA)

[b]Department of Chemical Engineering, Pennsylvania State University, University Park, PA 16802 (USA)

[c]Department of Physics, Pennsylvania State University, University Park, PA 16802 (USA)

*Benjamin J. Wiley (benjamin.wiley@duke.edu)
*Kristen A. Fichthorn (fichthorn@psu.edu)

Contents

Experimental Methods

Materials. Silver trifluoroacetate (CF_3COOAg, 98%), L-Ascorbic acid (AA, 99%), sodium trifluoroacetate (CF_3COONa, 98%), trifluoroacetic acid (CF_3COOH, 99%), polyvinylpyrrolidone (PVP, MW=10000, 29000, 55000, 360000, and 1300000), sodium citrate dihydrate ($Na_3CA{\cdot}2H_2O$, 99%), mercury thiocyanate ($Hg(SCN)_2$, 96.5%~103.5%), iron perchlorate hydrate ($Fe(ClO_4)_3{\cdot}xH_2O$) and perchloric acid ($HClO_4$, 70%) were obtained from Sigma-Aldrich. Ethylene glycol (99%) was obtained from J.T. Baker. Acetone was obtained from VWR Chemicals BDH. Silver nitrate ($AgNO_3$) and sodium chloride (NaCl) were obtained from Fisher Chemical. Sodium hydroxide (NaOH), sodium borohydride ($NaBH_4$), and hydrogen peroxide (H_2O_2, 30%) were obtained from EMD Millipore. Ammonium hydroxide (NH_4OH, 50%) and L-Arginine were obtained from Beantown Chemical. Hydrochloric acid (HCl, 37%) and PVP (MW=3500) were obtained from Acros Organics. Chromium(VI) Oxide (CrO_3, 99%) was obtained from Alfa Aesar. All the chemicals were used without further purification.

A silver-silver sulfate reference electrode (saturated K_2SO_4) was purchased from BASi Research Products. A platinum counter electrode was purchased from CH Instruments. Single-crystal silver electrodes were made from single-crystal silver disks (3.0 mm in diameter) purchased from Princeton Scientific based on a previous method.[1]

Synthesis of Truncated Silver Nanocubes as Single-Crystal Seeds. The synthesis of truncated silver nanocubes was based on a previous method with modifications.[1] First, 5.00 mL of ethylene glycol was added to a 250 mL double-neck flask preheated at 160 °C with a 20 cm condenser. A light nitrogen gas flow was applied above the solution for 10 minutes, followed by heating for another 50 minutes. After this, 2.96 mL of a solution containing 94.00 mM $AgNO_3$ in EG and 2.96 mL of a solution containing 144.0 mM PVP (MW=55,000) and 0.22 mM NaCl in EG

were simultaneously added to the flask at a rate of 45.0 mL/h. The reaction solution turned yellow immediately after the addition of the two solutions and gradually turned clear within 1 hour. The reaction solution turned light yellow again at about 3 hours and gradually deepens during the next 8 hours. At 12 hours, the reaction solution turned dark brown, gradually became greenish and finally turned ochre at 13 hours, indicating the reaction has been completed. The exact completion time of the reaction can vary between 11 hours to 15 hours. The reaction was quenched in an ice-water bath, 22.00 mL of acetone was added to the reaction solution, and this mixture was centrifuged at 2000 g for 30 minutes. The precipitate was washed with 10.00 mL of deionized water three additional times before dispersing it in 5 mL of deionized water.

Synthesis of Silver Decahedra as Penta-Twinned Seeds. The synthesis of silver decahedra was based on a previous method with modifications.[2] 70 mL deionized water, 2.6 mL of a 50 mM sodium citrate solution, 75 μL of a 50 mM PVP (MW=29,000) solution, 250 μL of a 5 mM arginine solution, 2.0 mL of a 5 mM silver nitrate solution, and 1.0 mL of a 100 mM sodium borohydride solution were added to a 250 mL beaker in sequence and the combined solution turned yellow after the addition of sodium borohydride. The solution was stirred in the dark for 50 minutes without visible color change. Following this, 1.6 mL of a 30% hydrogen peroxide solution was added, and the solution was stirred for another 20 minutes. After the addition of hydrogen peroxide, the solution would normally turn dark yellow within 7 minutes and the solution would bubble rapidly for a few minutes after the color change. After this, the beaker was capped with a petri dish and a blue light lamp (18 W BlueX LED) placed 60 cm above the solution was turned on. The solution was stirred for another 14 hours under the blue light. Then, the reaction solution was centrifuged at 10,000 rpm for 25 minutes, and the precipitate was washed with 10 mL of ice-cold

deionized water once. The product was dispersed in 5 mL of deionized water, stored in an ice bath and immediately used for seed-mediated growth.

Seed-Mediated Growth. For a typical synthesis with 30 mM PVP (MW=29,000) and 6 μM Cl^-, 2 mL of a 2.4 mM ascorbic acid solution, 1 mL of an 11.88 mM sodium trifluoroacetate solution, 1 mL of a 1.92 mM trifluoroacetic acid solution, 1 mL of a 360 mM PVP (MW=29,000) solution, 1 mL of a 72 μM NaCl solution, and 2 mL of seeds were first mixed. For the seed suspension containing truncated silver nanocubes, 0.06 mL of as-prepared seeds were diluted to 2 mL with water. For the seed suspension containing silver decahedra, 0.05 mL of as-prepared seeds were diluted to 2 mL with water. Following this, 4 mL of a 0.6 mM silver trifluoroacetate solution was added. The solution was stirred for 13 minutes and then centrifuged at 10,000 rpm for 4 minutes. The precipitate was washed with 7 mL of deionized water for three times and centrifuged at 10,000 rpm for 4 min. The product was dispersed in 0.5 mL of deionized water for imaging. Syntheses with other PVP and Cl^- concentrations were performed in the same manner except the concentrations of PVP and NaCl were changed, and the preparation of growth solutions under different conditions can be found in **Table S2**.

Scanning Electron Microscopy (SEM). SEM images were obtained with a Apreo S scanning electron microscope (ThermoFisher Scientific). The single-crystal silver nanocrystals were imaged at an accelerating voltage of 2.0 kV and a beam current of 25 pA. The penta-twinned silver nanocrystals were imaged at an accelerating voltage of 10.0 kV and a beam current of 50 pA. The samples were prepared by dropping 2~10 μL of the sample solutions on a piece of silicon followed by drying in air.

Transmission Electron Microscopy (TEM). The TEM images were obtained with a transmission electron microscope (FEI Tecnai G^2 Twin) operated at an accelerating voltage of 160

kV. Samples were prepared by dropping 8 μL of the sample solution on 300 mesh carbon-coated copper grids (Pacific Grid-Tech). The excess solution was removed with filter paper after 1 min, and the grid was dried in the open air before imaging.

Electrochemical Measurements. The single-crystal silver electrodes were prepared based on a modified etching method.[1] The Ag(100) and Ag(111) electrodes (3mm in diameter) were first mechanically polished with alumina powder (0.3 μm) until they appeared to have mirror-like surfaces. Then, each of the electrodes was dipped in three stirred solutions (1) chromium trioxide (0.15 M) and hydrochloric acid (0.1 M) for 1 minute, (2) 50% ammonium hydroxide for 5 minutes, and (3) trifluoroacetic acid (4 M) for 2 minutes. The electrodes were thoroughly rinsed with a flow of deionized water and dried with a flow of nitrogen gas after etching in each solution.

The facet-selectivity of PVP and chloride was measured by performing Linear Sweep Voltammetry (LSV) in the growth solution for the seeds. The seed-mediated growth occurred too quickly for electrochemical analysis of the mixed reaction solution (the reaction was complete in 13 minutes), so the rate of silver ion reduction and ascorbic acid oxidation at the mixed potential were analyzed separately, i.e., in solutions containing no ascorbic acid and no silver ions, respectively. LSV was performed from -0.28V to -0.03V at a rate of 5 mV/s with one polished single-crystal silver electrode as a working electrode, an Hg/Hg_2SO_4 electrode (saturated K_2SO_4) as a reference electrode and a platinum wire as a counter electrode. Each solution was stirred for 2 minutes before the electrodes were placed into the solution, and the electrodes were held in the solution for 2 minutes before starting the LSV scan. The solutions were constantly stirred at 500 rpm during the measurement. The concentrations of additives in the solutions that were analyzed are summarized in **Table S2**.

Quantification of Cl^- Contamination in PVP. The amount of Cl^- (halide) contamination in PVP was measured based on a previous method with modifications.[3] The method is based on the fact that halides, such as Cl^- and Br^-, can displace SCN^- from $Hg(SCN)_2$. The released SCN^- further reacts with Fe^{3+} to form a red complex, making it possible to determine the halide concentration by measuring the absorption of the red Fe(III) complex.

All solutions were prepared with water as a solvent. A saturated $Hg(SCN)_2$ solution was prepared by adding 0.1 g of $Hg(SCN)_2$ to 40 mL of deionized water. After 24 hours, the mixture was centrifuged at 10,000 rpm for 10 minutes twice, and the supernatant was transferred to a clean centrifuge tube to be used as the saturated $Hg(SCN)_2$ solution. Deionized water, and 0.2 mM, 0.4 mM, 0.8 mM NaCl solutions were used as standard solutions. To measure the absorption spectrum at different Cl^- concentrations, 0.6 mL of a standard solution and 0.6 mL of a 6% $Fe(ClO_4)_3 \cdot xH_2O$ in 4 M $HClO_4$ solution were first mixed. After this, 0.3 mL of a saturated $Hg(SCN)_2$ solution was added. The solution was thoroughly mixed, and its UV-Vis spectrum from 700 nm to 350 nm was collected with a Shimadzu UV-3600i spectrophotometer. A calibration curve was generated with the absorbances at 460 nm.

PVP of different MWs were measured in the same manner, except the solutions need to be centrifuged since the addition of a 6% $Fe(ClO_4)_3 \cdot xH_2O$ in 4 M $HClO_4$ solution to 1 ~ 2.5 M PVP will cause PVP to aggregate. For 2-pyrrolidone and PVP with MWs of 29000 and 55000, 1.5 mL of a 2.5 M PVP (or 2-Pyrrolidone) solution and 1.5 mL of a 6% $Fe(ClO_4)_3 \cdot xH_2O$ in 4 M $HClO_4$ solution were first mixed and centrifuged at 3000 rpm for 10 minutes to remove excess PVP. After this, 1.2 mL of the supernatant was transferred to a glass cuvette, and 0.3 mL of a saturated $Hg(SCN)_2$ solution was added. The solution was thoroughly mixed, and its UV-Vis spectrum from 700 nm to 350 nm was measured. For PVP with MWs of 3500 and 10000, 1.5 mL of a 2.5 M PVP

solution and 1.5 mL of a 6% $Fe(ClO_4)_3 \cdot xH_2O$ in 4 M $HClO_4$ solution were first mixed and centrifuged at 10,000 rpm for 10 minutes. After this, 1.2 mL of the supernatant was transferred to a clean centrifuge tube, and 0.3 mL of a saturated $Hg(SCN)_2$ solution was added. The solution was thoroughly mixed, and if the solution is cloudy, centrifuge the solution at 10,000 rpm for 10 minutes. The supernatant was transferred to a glass cuvette to obtain its UV-Vis spectrum. For PVP with MWs of 360000 and 1300000, 1.5 mL of a 1.0 M PVP solution and 1.5 mL of a 6% $Fe(ClO_4)_3 \cdot xH_2O$ in 4 M $HClO_4$ solution were first mixed and centrifuged at 3000 rpm for 10 minutes to remove excess PVP. After this, 1.2 mL of the supernatant was transferred to a glass cuvette, and 0.3 mL of a saturated $Hg(SCN)_2$ solution was added. The solution was thoroughly mixed, and its UV-Vis spectrum was collected. PVP of each MW was measured twice to determine the amount of halide contamination.

To extract the absorption spectrum only originated from the Fe^{3+}-SCN^- complex, background absorption needs to be removed from the measured spectra. For 2-pyrrolidone and PVP with MWs of 3500 and 10000, the background solutions were prepared in the same manner as the above-mentioned procedure except 0.3 mL of saturated $Hg(SCN)_2$ solution was replaced with 0.3 mL of water. The background solutions were yellow after centrifugation for these samples. For PVP with MWs of 29000-1300000, the raw absorption spectrum of 0 mM NaCl standard spectrum was used as the background. A baseline based on the absorbance at 700 nm was further removed from the spectra for these samples. The background corrected spectra were shown in **Figure S2** and the results were summarized in **Table S1**.

Determination of *R* for a Penta-Twinned Decahedron and a Rod. A silver decahedron is comprised of five single-crystal silver tetrahedra grouped along one same axis along the ⟨110⟩ direction (**Figures S7A and S7B**). When observed from the top, each decahedron occupies 70.6°

of the space around the ⟨100⟩ axis. This geometry theoretically leaves 7.0° of gaps between the twin planes.

When a small decahedron with an edge length of a_1 grows into a large decahedron with an edge length of a_2, the growth leads to a dimensional change in the ⟨100⟩ direction, $d_2 - d_1$ (**Figure S7C**). Based on the geometry of a decahedron,

$$d_2 - d_1 = (a_2 - a_1)\cot 35.3° \quad . \tag{S1}$$

The growth also leads to a dimensional change in the ⟨111⟩ direction, $h_2 - h_1$, which can be calculated by either of the following two ways. (1) Since the angle between ⟨111⟩ and ⟨100⟩ is 54.7°,

$$h_2 - h_1 = (d_2 - d_1)\cos 54.7° = (a_2 - a_1)\cot 35.3° \cos 54.7° \quad . \tag{S2}$$

(2) Since the dimensional change in the ⟨110⟩ direction, $L_2 - L_1$, is the same as the edge length change, $a_2 - a_1$, and the angle between ⟨111⟩ and ⟨110⟩ is 35.3°,

$$h_2 - h_1 = (L_2 - L_1)\cos 35.3° = (a_2 - a_1)\cos 35.3° \quad . \tag{S3}$$

Given that $\cot 35.3° \cos 54.7° = \cos 35.3°$, the two methods reach the same result. The ratio *R* of atomic deposition along ⟨100⟩ and ⟨111⟩ can be calculated by

$$R = \frac{d_2 - d_1}{h_2 - h_1} = \frac{(a_2 - a_1)\cot 35.3°}{(a_2 - a_1)\cos 35.3°} = 1.73 \quad . \tag{S4}$$

Note that there are only {111} facets and no {100} facets on the decahedron surfaces.

When *R* is smaller than 1.73, decahedra grow into rods. When the rods are characterized by SEM, we assume the rods rest on one of the five side rectangular facets and the measured width (*W*) is the projection perpendicular to the rested facet (**Figure S8**).

The dimensional change in *W* can be calculated from the top view projection edge length, *a*, which is dependent on the atomic deposition rate along the ⟨100⟩ direction, $rate_{\langle 100 \rangle}$. Based on the geometry of the rods,

$$dW = da\frac{\sin 108^\circ}{\sin 35.3^\circ} = rate_{<100>}dt \tan 35.3^\circ \frac{\sin 108^\circ}{\sin 35.3^\circ} \quad . \quad \text{(S5)}$$

The dimensional change in L is dependent on the atomic deposition rate along the $\langle 111 \rangle$ direction, $rate_{\langle 111 \rangle}$. Based on the geometry of the front-viewed rods,

$$dL = rate_{<111>}dt \sin 54.7^\circ \quad . \quad \text{(S6)}$$

Therefore,

$$\frac{dW}{dL} = \frac{rate_{<100>} \tan 35.3^\circ \sin 108^\circ}{rate_{<111>} \sin 54.7^\circ \sin 35.3^\circ} = 1.44R \quad , \quad \text{(S7)}$$

and

$$R = 0.694\frac{dW}{dL} \quad . \quad \text{(S8)}$$

Theoretical Methods

DFT Calculations. In this work, we represent PVP as divinylpyrrolidone (DVP), an isotactic dimer of PVP monomer (**Figure S10**). To probe the surface structures of Cl^- and DVP on Ag(100) and Ag(111), Cl^- coverages ranging from 0.00 monolayer (ML) to a maximum of 0.5 ML on both Ag surfaces were tested with a DVP coverage of either 0.063 ML or 0.11 ML. From MD simulation results,[4] we assumed the ideal situation, in which most water solvent molecules would not pass through the DVP adlayer on the Ag surfaces. As a result, we did not include water explicitly in this work.

All DFT calculations in this work were performed using the Vienna *Ab initio* Simulation Package (VASP) projector-augmented wave pseudopotential method.[5-9] The generalized gradient approximation with the Perdew, Burke, and Ernzerhof (PBE) exchange-correlation functional was applied.[10] In the DFT calculations, the optimization criteria were set to be 0.01 eV/Å for forces in the ionic steps and 10^{-6} eV for the self-consistent energy in the electronic steps. The energy cutoff for the plane-wave basis set was 450 eV. A Methfessel–Paxton smearing of 0.1 eV was applied

for all calculations and Monkhorst-Pack grids were used for integration over the first Brillouin zone. Different unit cells were used for different coverages of Cl^- and DVP, in which a (3×3) unit cell is the minimum based on the size of DVP. For bulk Ag calculations, a $(15 \times 15 \times 1)$ $\boldsymbol{k}$-point mesh was used. A cubic cell with a dimension of 25 Å was used for calculations of a DVP dimer in vacuum. To model adsorption on Ag surfaces, a six-layer Ag slab with Cl^- and/or DVP adsorbed on one side of the topmost layer was employed. A large enough vacuum space was introduced between the two periodic unit cells along the surface normal to avoid interactions between neighboring unit cells, as shown in the convergence tests (**Table S3**). During structural optimization, the upper three layers with all adsorbed species were fully relaxed and the bottom three layers of the slab were kept fixed at the Ag bulk positions with a lattice constant of 4.092 Å. A dipole correction was applied in the normal direction to the slab.

To account for long-range interactions, which contribute greatly in this metal-organic adsorption system, we applied the DFT-D2 dispersion correction by Grimme to introduce van der Waals (vdW) interactions.[11] A cutoff radius of 40.00 Å was employed for the vdW interaction and the C_6 and R_0 parameters from the work by Ruiz *et al.* were used for Ag to account for the screening effect of bulk Ag,[12] while all other parameters were the default values from Grimme's DFT-D2 method.

Several energetic characteristics were calculated to identify different configurations of DVP and/or Cl^- on the Ag surfaces. The binding energy of DVP E_{bind} is given by

$$E_{\mathrm{bind}} = (N_{\mathrm{DVP}}E_{\mathrm{DVP}} + E_{\mathrm{slab}} - E_{\mathrm{Sys}})/N_{\mathrm{DVP}} \quad . \tag{S9}$$

Here, N_{DVP} is number of DVP molecules in the unit cell and E_{DVP} is the optimal energy of one isolated DVP molecule in the gas phase. E_{slab} is the optimal energy of an Ag (or Ag with adsorbed Cl) slab, and E_{Sys} is the total energy of the optimal adsorption system (Ag slab + adsorbed Cl +

adsorbed DVP). The binding energy can be decomposed into short-range interactions, arising from direct chemical bonding and Pauli repulsion ($E_{\mathrm{bind}}^{\mathrm{short}}$) and the long-range vdW interaction ($E_{\mathrm{bind}}^{\mathrm{vdW}}$), such that $E_{\mathrm{bind}} = E_{\mathrm{bind}}^{\mathrm{short}} + E_{\mathrm{bind}}^{\mathrm{vdW}}$. Each of these two components has contributions from DVP-Ag, DVP-DVP, and Ag surface interactions, as discussed elsewhere.[13, 14] The surface energy of an Ag surface containing adsorbed Cl and DVP, $\gamma_{\mathrm{Ag-Cl-DVP}}$, is given by

$$\gamma_{\mathrm{Ag-Cl-DVP}} = \frac{E_{\mathrm{Sys}} - N_{\mathrm{Ag}} E_{\mathrm{Ag,bulk}} - N_{DVP}\,\mu_{DVP} - N_{\mathrm{Cl^-}}\mu_{\mathrm{Cl^-}}}{A_{\mathrm{slab}}} - \gamma_{\mathrm{fixed}} \quad . \tag{S10}$$

Here, $E_{\mathrm{Ag,bulk}}$ is the energy of one Ag atom in bulk and N_{Ag} is the number of Ag atoms in the slab. $N_{\mathrm{Cl^-}}$ and $\mu_{\mathrm{Cl^-}}$ represent the number of chloride atoms in the unit cell and the chloride chemical potential, respectively, while N_{DVP} and μ_{DVP} are the number of DVP dimers and the chemical potential for a DVP dimer. A_{slab} is the surface area of one side of the slab and γ_{fixed} is the surface energy of the fixed side of the slab. γ_{fixed} is given by

$$\gamma_{\mathrm{fixed}} = (E_{\mathrm{Ag}} - N_{\mathrm{Ag}} E_{\mathrm{Ag,bulk}})/2A_{\mathrm{slab}} \quad , \tag{S11}$$

where E_{Ag} is the energy of a bare Ag slab with atoms fixed at the bulk coordinates.

Supplementary Tables

Table S1. Cl^- contamination in 2-pyrrolidone and PVP of different MWs

PVP MW	Cl^- Contamination	Cl^- Contamination per 30 mM PVP
2-Pyrrolidone	0.0246 ± 0.0025 mM in 2.5 M 2-Pyrrolidone	0.2952 ± 0.0305 µM
3,500	0.7729 ± 0.0205 mM in 2.5 M PVP	9.2758 ± 0.2461 µM
10,000	0.0232 ± 0.0008 mM in 2.5 M PVP	0.2790 ± 0.0093 µM
29,000	0.0172 ± 0.0013 mM in 2.5 M PVP	0.2070 ± 0.0161 µM
55,000	0.0277 ± 0.0024 mM in 2.5 M PVP	0.3324 ± 0.0029 µM
360,000	0.0206 ± 0.0005 mM in 1.0 M PVP	0.6195 ± 0.0148 µM
1,300,000	0.0042 ± 0.0027 mM in 1.0 M PVP	0.1260 ± 0.0806 µM

Table S2. Concentrations of additives for synthetic or electrochemical experiments.

[PVP]/mM	[Cl^-]/μM	[CF_3COONa]/mM	[CF_3COOH]/mM	[AA]/mM	[CF_3COOAg]/mM	Figures
0	0	11.88	1.92	0.4	0.2	1C, 3A, S9A
0	0.6	11.88	1.92	0.4	0.2	S4A, S3B, S9B
0	1.2	11.88	1.92	0.4	0.2	S4B
0	6	11.88	1.92	0.4	0.2	1E, 3C, 5C
0	12	11.88	1.92	0.4	0.2	S4C
0	60	11.88	1.92	0.4	0.2	S4D, S9C
0.003	0	11.88	1.92	0.4	0.2	S5A
0.003	6	11.88	1.92	0.4	0.2	S3E, S5E
0.03	0	11.88	1.92	0.4	0.2	S5B
0.03	6	11.88	1.92	0.4	0.2	S5F
0.3	0	11.88	1.92	0.4	0.2	S3A, S5C
0.3	6	11.88	1.92	0.4	0.2	S3C, S5G
3	0	11.88	1.92	0.4	0.2	S5D
3	6	11.88	1.92	0.4	0.2	S5H
30	0	11.88	1.92	0.4	0.2	1D, 3B, 5D
30	0.6	11.88	1.92	0.4	0.2	5E, S3D, S4E
30	1.2	11.88	1.92	0.4	0.2	S4F
30	1.8	11.88	1.92	0.4	0.2	S6A
30	3	11.88	1.92	0.4	0.2	S6B
30	6	11.88	1.92	0.4	0.2	1F, 3D, 5F
30	12	11.88	1.92	0.4	0.2	S4G
30	60	11.88	1.92	0.4	0.2	S3F, S4H

Table S3. Results of convergence tests on the total binding energy per DVP molecule (in eV) for various ***k***-point sampling, energy cutoff, and vacuum spacing. Values in the shaded cells were used to obtain the final results. E_{bind} is given by **Equation S9**.

k-point					
$\mathrm{Ag}(100)-(3\times3)$ *	$(5\times5\times1)$	$(6\times6\times1)$	$(7\times7\times1)$	$(8\times8\times1)$	$(9\times9\times1)$
E_{bind} (eV)	1.12	1.13	1.13	1.13	1.13
$\mathrm{Ag}(100)-(4\times4)$ *	$(4\times4\times1)$	$(5\times5\times1)$	$(6\times6\times1)$	$(7\times7\times1)$	$(8\times8\times1)$
E_{bind} (eV)	0.92	0.91	0.90	0.91	0.91
Energy cutoff (eV) *	400.00	450.00	500.00	550.00	600.00
E_{bind} (eV)	1.13	1.13	1.12	1.12	1.12
Vacuum spacing (Å)*	37.00	38.00	39.00	40.00	41.00
E_{bind} (eV)	1.12	1.13	1.13	1.13	1.13

* Choices of ***k***-point sampling for Ag(111) are made based on the results of Ag(100). Tests on energy cutoff and vacuum spacing are based on the $\mathrm{Ag}(100)-(3\times3)$ unit cell.

Table S4. Binding energies (in eV) and distances between each of the two O atoms and the nearest Ag (in Å) for different adsorption configurations of DVP on Ag(100) and Ag(111) at 0.11 ML coverage. E_{bind} is given by **Equation S9**.

Surface	Conformation Number	E_{bind}	$d^{1}_{\mathrm{O-Ag}}$	$d^{2}_{\mathrm{O-Ag}}$
Ag(100)	1	1.13	2.50	3.05
	2	1.03	2.56	2.72
	3	0.99	2.64	2.84
	4	0.83	2.61	2.63
Ag(111)	1	1.06	2.63	2.84
	2	1.02	2.86	2.87
	3	1.06	2.61	2.80
	4	1.05	2.64	2.87

Table S5. Binding energies (in eV) of the optimal adsorption configurations of DVP on Ag(100) and Ag(111) at different Cl^- and DVP coverages (in ML). E_{bind} is given by **Equation S9**. The decomposition of E_{bind} into short-range ($E_{\mathrm{bind}}^{\mathrm{short}}$) and vdW ($E_{\mathrm{bind}}^{\mathrm{vdW}}$) interactions, as well as the short-range $\left(E_{\mathrm{DVP-Ag}}^{\mathrm{short}}\right)$ and vdW ($E_{\mathrm{DVP-Ag}}^{\mathrm{vdW}}$) components of the molecule-surface interactions are also shown.

Surface	Cl^- Coverage	DVP Coverage	E_{bind}	$E_{\mathrm{bind}}^{\mathrm{short}}$	$E_{\mathrm{bind}}^{\mathrm{vdW}}$
Ag(100)	0.00	0.11	1.127	0.106	1.022
	0.063	0.063	1.109	0.189	0.920
	0.11	0.11	1.416	0.226	1.191
	0.22	0.11	1.617	0.276	1.341
	0.25	0.063	1.618	0.438	1.180
	0.33	0.11	1.549	0.205	1.344
	0.438	0.063	1.359	0.116	1.243
	0.50	0.11	0.908	-0.542	1.450
Ag(111)	0.00	0.11	1.062	-0.159	1.221
	0.063	0.063	1.182	0.155	1.027
	0.11	0.11	1.448	0.106	1.342
	0.22	0.11	1.547	0.131	1.415
	0.25	0.063	1.814	0.552	1.262
	0.33	0.11	1.285	-0.225	1.51
	0.438	0.063	1.067	0.056	1.011
	0.50	0.11	0.644	0.085	0.559

Table S6. Coverages of Cl^- and DVP on Ag(100) and Ag(111) in each numbered region of **Figure S15**.

Coverage / Region	Ag(100)		Ag(111)	
	Cl^- (ML)	DVP (ML)	Cl^- (ML)	DVP (ML)
1	-	-	-	-
2	1/16	-	-	-
3	1/4	-	-	-
4	1/4	1/16	-	-
5	2/9	1/9	-	-
6	1/9	1/9	-	-
7	-	1/9	-	-
8	-	1/9	-	1/9
9	1/9	1/9	-	1/9
10	1/9	1/9	1/9	1/9
11	2/9	1/9	1/9	1/9
12	2/9	1/9	2/9	1/9
13	2/9	1/9	1/4	1/1

Supplementary Figures

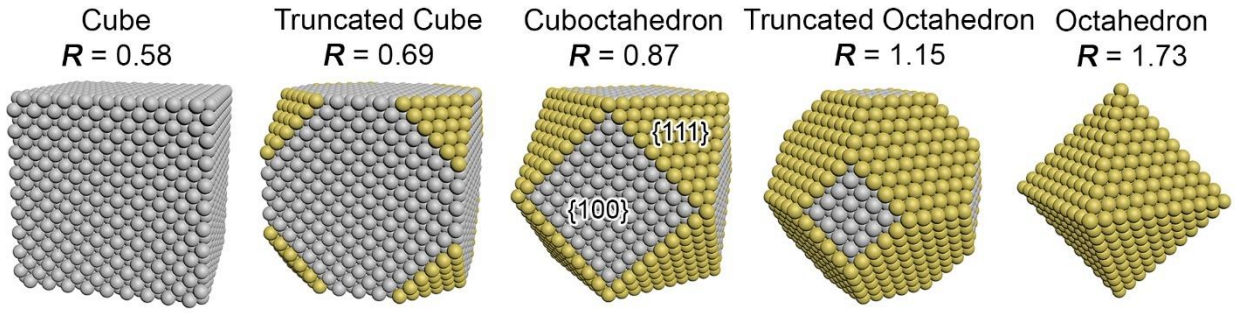

Figure S1. Schematic representation of the single-crystal Ag nanocrystals formed at different ratio (R) of growth rates along ⟨100⟩ and ⟨111⟩.[1]

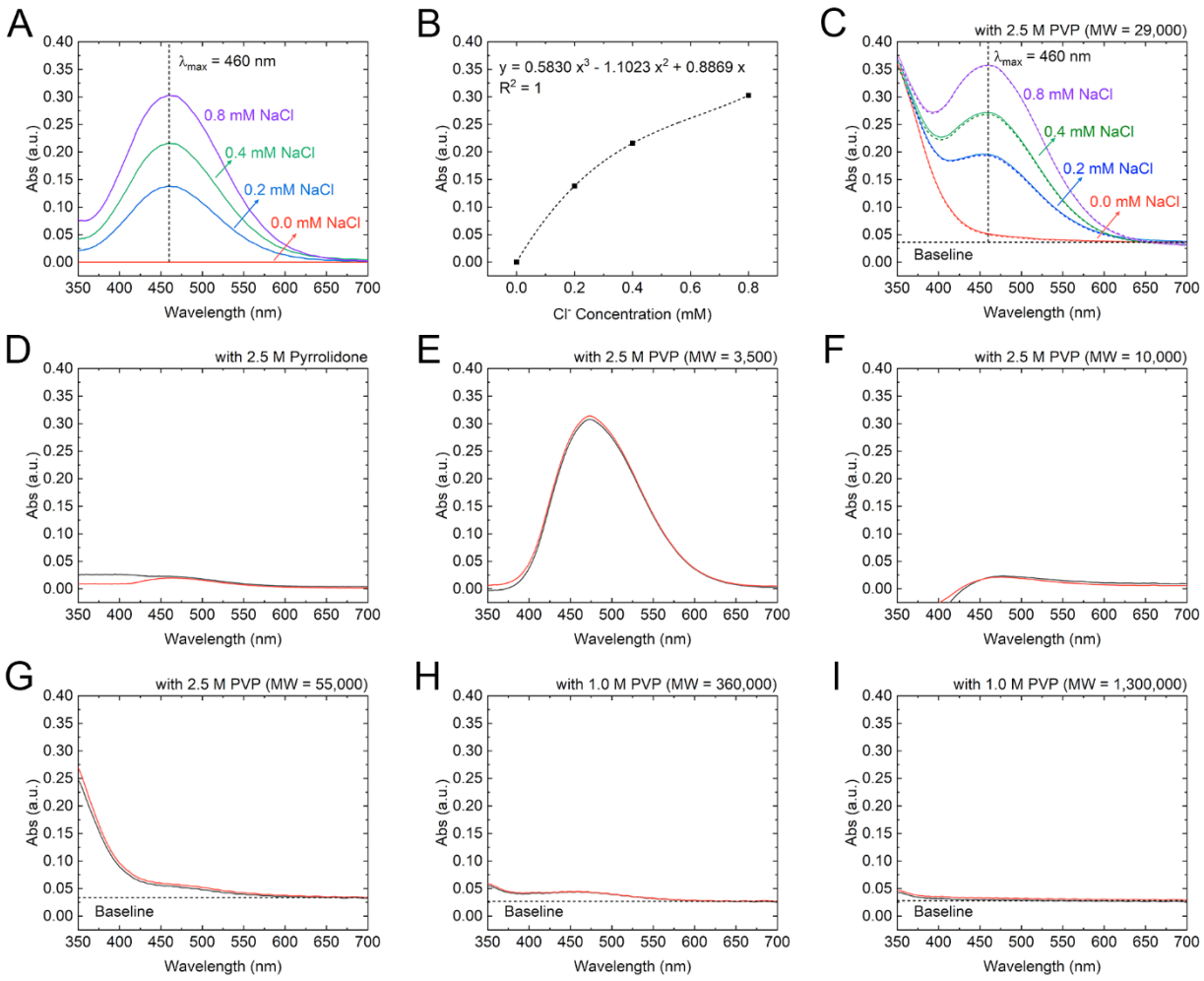

Figure S2. Measurements of Cl^- contamination in PVP. (A) UV-Vis spectra of the Cl^- test solutions with the addition of different amounts of NaCl. (B) Absorbances at λ_{max}= 460 nm at different Cl^- concentrations. (C) UV-Vis spectra of the Cl^- test solutions with the addition of 2.5 M PVP (MW=29,000) and the addition of different amounts of NaCl. (D-I) UV-Vis spectra of the Cl^- test solutions with the addition of 2-pyrrolidone or PVP of different MWs. (D) 2.5 M 2-pyrrolidone, (E) 2.5 M PVP (MW=3,500), (F) 2.5 M PVP (MW=10,000), (G) 2.5 M PVP (MW=55,000), (H) 1.0 M PVP (MW=360,000) and (I) 1.0 M PVP (MW=1,300,000).

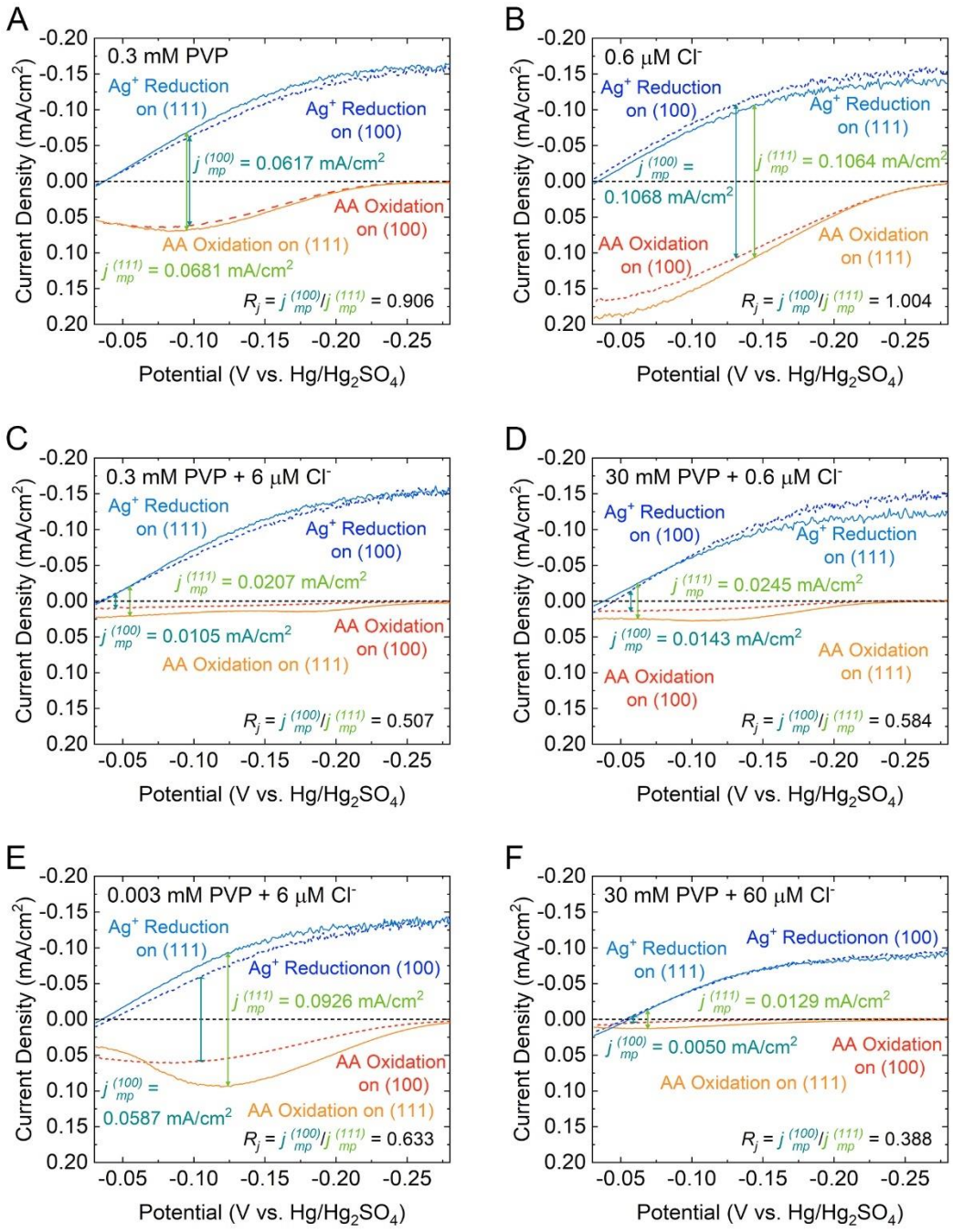

Figure S3. LSVs for Ag^+ reduction and AA oxidation half-reactions on Ag(100) and Ag(111) electrodes with (A) 0.3 mM PVP, (B) 0.6 μM Cl^-, (C) 0.3 mM PVP and 6 μM Cl^-, (D) 30 mM PVP and 0.6 μM Cl^-, (E) 0.003 mM PVP and 6 μM Cl^-, and (F) 30 mM PVP and 60 μM Cl^-,

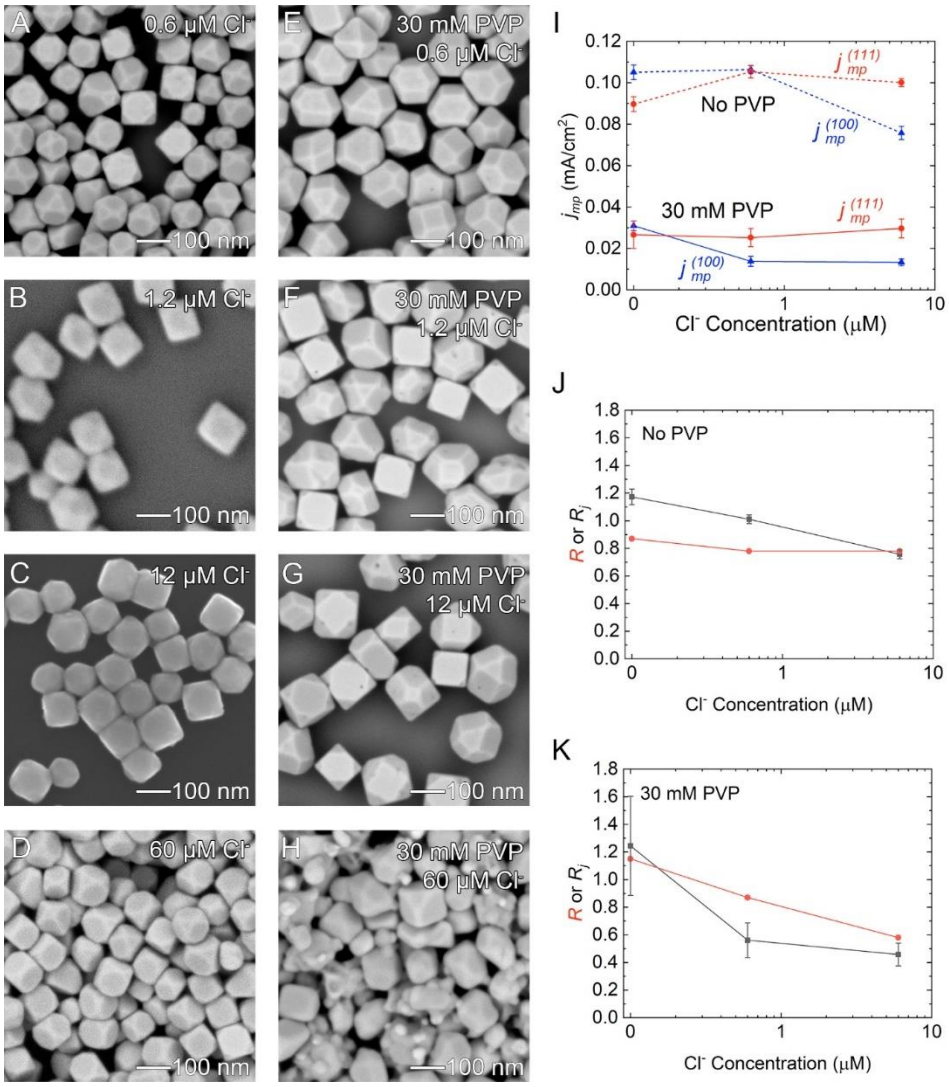

Figure S4. (A-D) SEM images of the silver nanocrystals grown from the single-crystal seeds in the presence of no PVP and different concentrations of Cl^-. (A) 0.6 μM, (B) 1.2 μM, (C) 12 μM and (D) 60 μM. (E-H) SEM images of the silver nanocrystals grown from the single crystal seeds in the presence of 30 mM PVP and different concentrations of Cl^-. (E) 0.6 μM, (F) 1.2 μM, (G) 12 μM and (H) 60 μM. (I) $j_{mp}^{(100)}$ and $j_{mp}^{(111)}$ in the presence of different concentrations of Cl^-. (J) R (growth along ⟨100⟩/⟨111⟩) and R_j ($j_{mp}^{(100)}/j_{mp}^{(111)}$) in the absence of PVP and the presence of different concentrations of Cl^-. (K) R (growth along ⟨100⟩/⟨111⟩) and R_j ($j_{mp}^{(100)}/j_{mp}^{(111)}$) in the presence of 30 mM PVP and different concentrations of Cl^-.

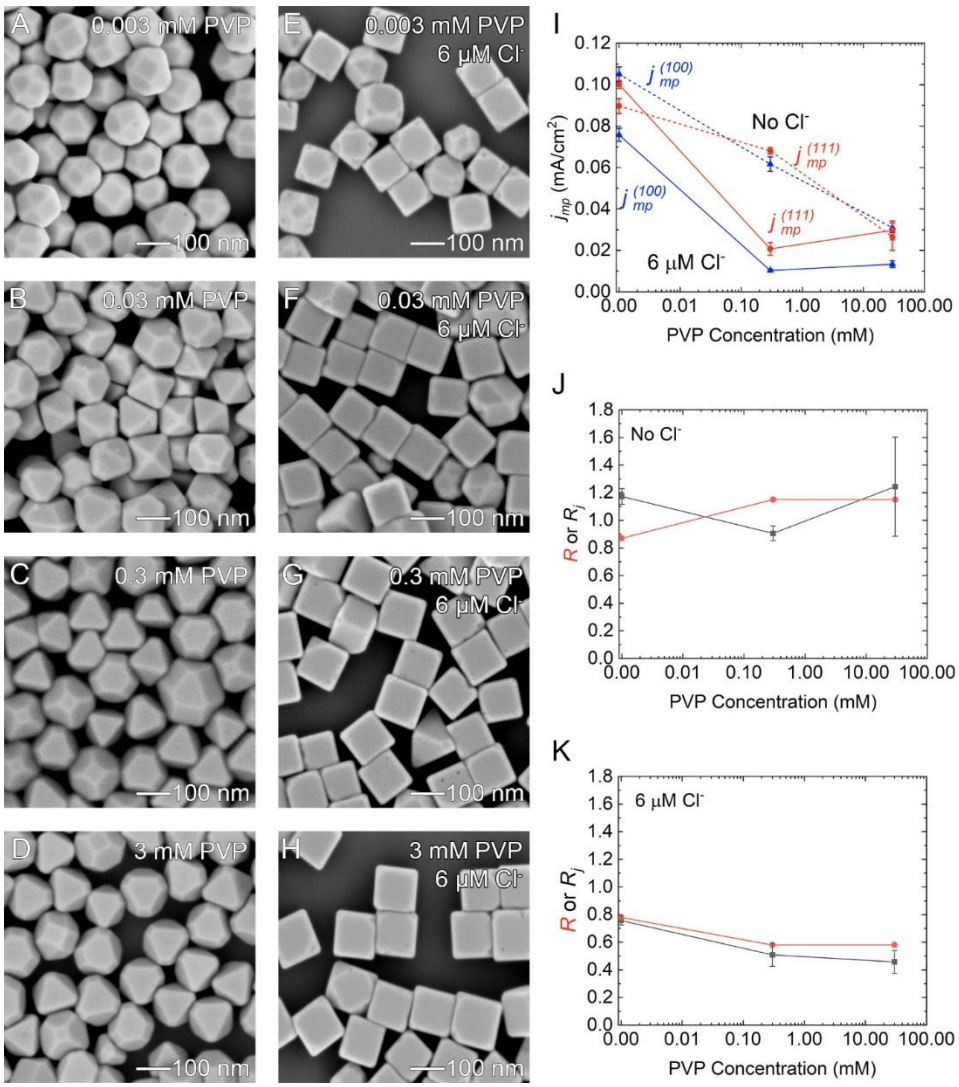

Figure S5. (A-D) SEM images of the silver nanocrystals grown from the single-crystal seeds in the presence of no Cl^- and different concentrations of PVP. (A) 0.003 mM, (B) 0.03 mM, (C) 0.3 mM and (D) 3 mM. (E-H) SEM images of the silver nanocrystals grown from the single crystal seeds in the presence of 6 μM Cl^- and different concentrations of PVP. (E) 0.003 mM, (F) 0.03 mM, (G) 0.3 mM and (H) 3 mM. (I) $j^{(100)}_{mp}$ and $j^{(111)}_{mp}$ in the presence of different concentrations of PVP. (J) R (growth along $\langle 100 \rangle / \langle 111 \rangle$) and R_j ($j^{(100)}_{mp}/j^{(111)}_{mp}$) in the absence of Cl^- and the presence of different concentrations of PVP. (K) R (growth along $\langle 100 \rangle / \langle 111 \rangle$) and R_j ($j^{(100)}_{mp}/j^{(111)}_{mp}$) in the presence of 6 μM Cl^- and different concentrations of PVP.

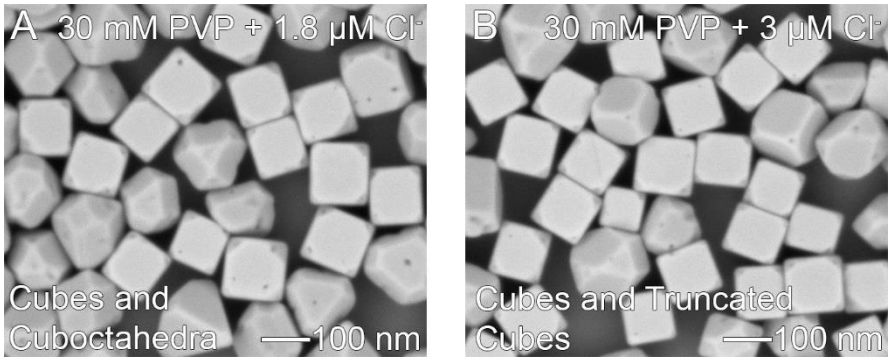

Figure S6. SEM images of the silver nanocrystals grown from the single-crystal seeds in the presence of 30 mM PVP and different concentrations of Cl^-. (A) 1.8 μM Cl^- and (B) 3 μM Cl^-.

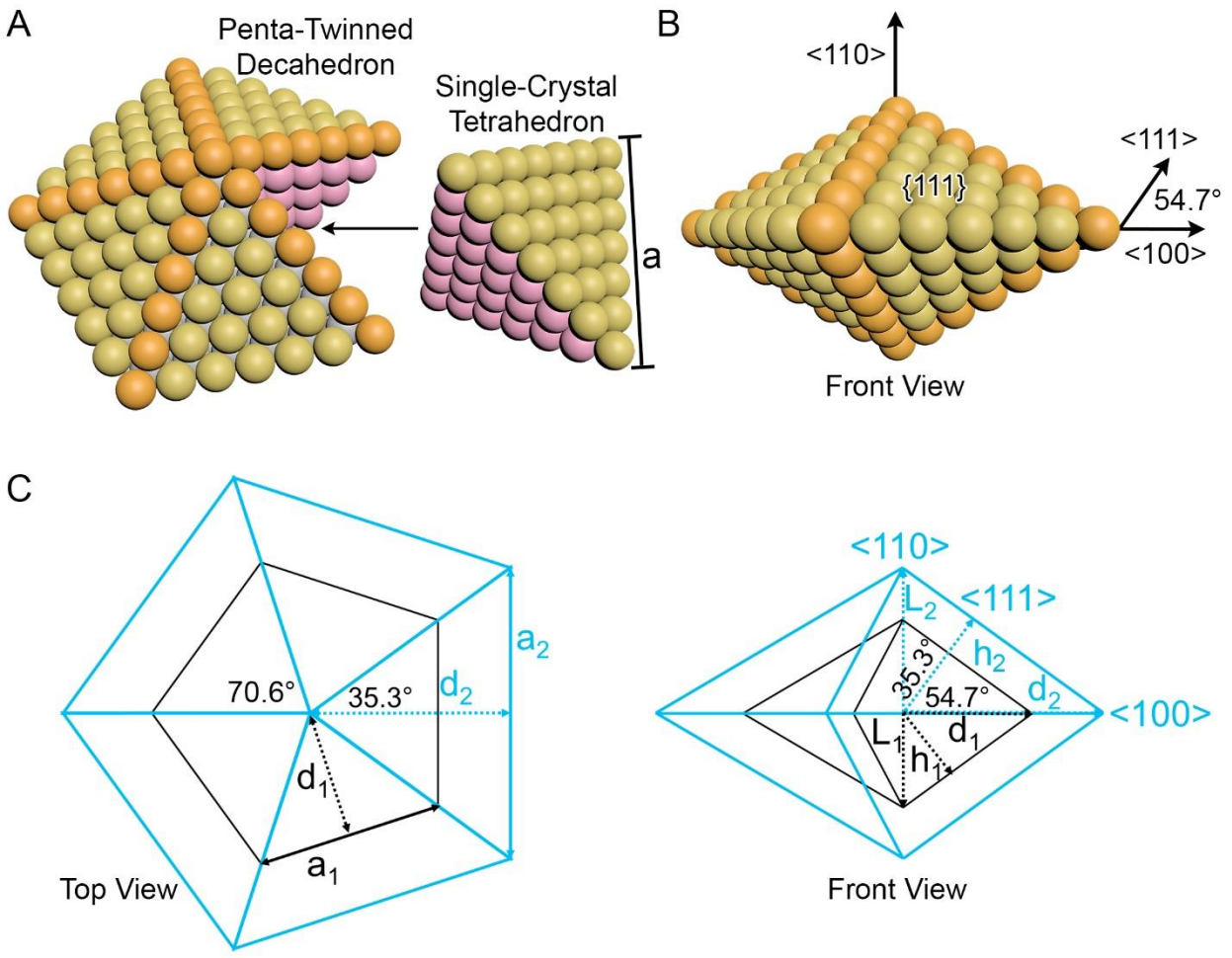

Figure S7. (A) Schematic representation of an Ag decahedron that is comprised of five single-crystal Ag tetrahedra grouped along one same axis. Orange indicates the surface atoms of the twin planes, and pink indicates the inner atoms of the twin planes. (B) Crystal facets and directions of an Ag decahedron. (C) Schematic illustration to accompany the discussion of how to calculate the ratio R of growth along the <100> and <111> directions when a small decahedron grows into a large decahedron.

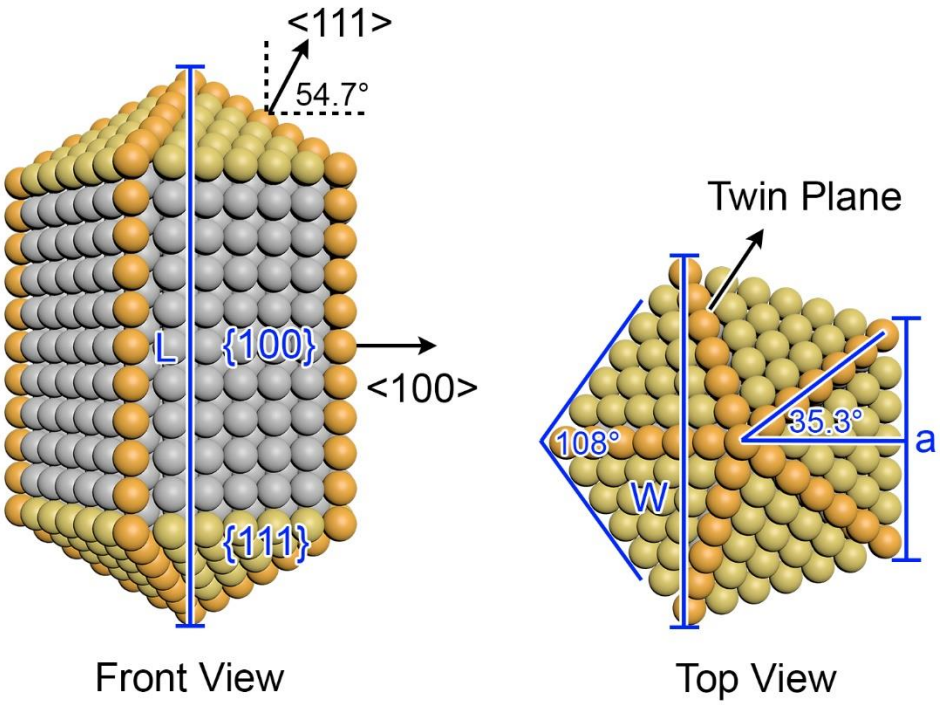

Figure S8. Schematic representation of an Ag nanorod and its crystal facets and directions.

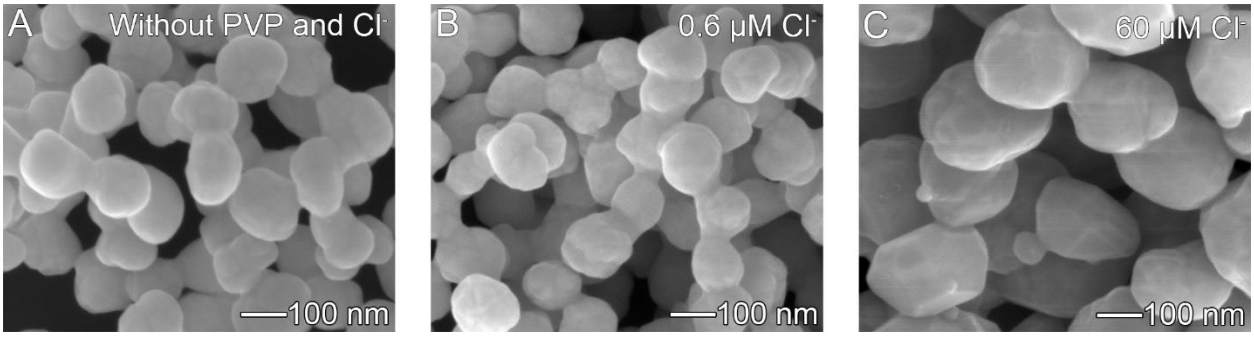

Figure S9. SEM images of the silver nanocrystals grown from the decahedron seeds in the presence of (A) no PVP and Cl^-, (B) 0.6 μM Cl^- and (C) 60 μM Cl^-.

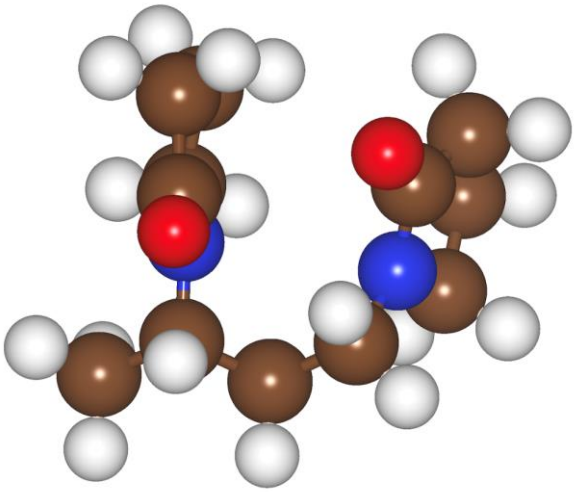

Figure S10. Optimized configuration of the isotactic DVP dimer in the gas phase. (Red: O, Blue: N, Brown: C, and White: H).

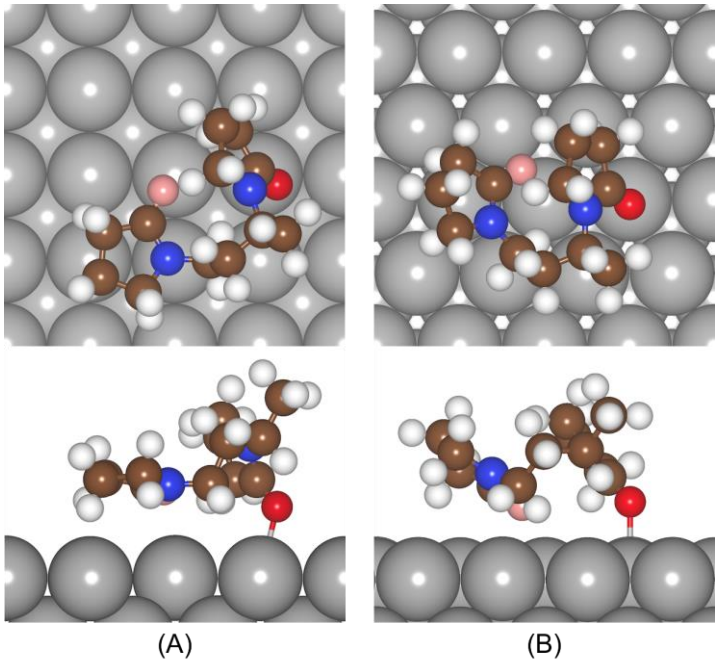

Figure S11. Optimal binding conformations of DVP on Ag – conformation (1) in **Table S4**. Top-down (upper) and side (lower) views of the optimal binding conformations at 0.11 ML DVP coverage with the highest binding energy on **(A)** Ag(100) and **(B)** Ag(111) (Gray: Ag, Red: bound O, Pink: unbound O, Blue: N, Brown: C, and White: H).

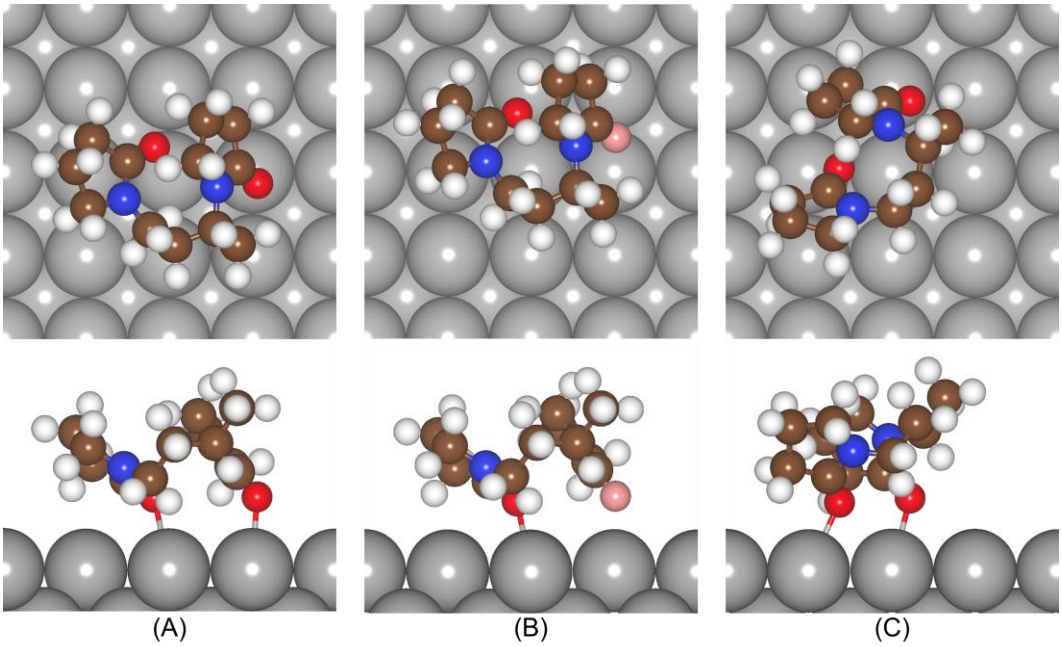

Figure S12. Binding conformations of DVP on Ag(100). Top-down (upper) and side (lower) views of DVP at 0.11 ML coverage on Ag(100) with binding conformation (**A**) 2, (**B**) 3, and (**C**) 4 in **Table S4** (Gray: Ag, Red: bound O, Pink: unbound O, Blue: N, Brown: C, and White: H).

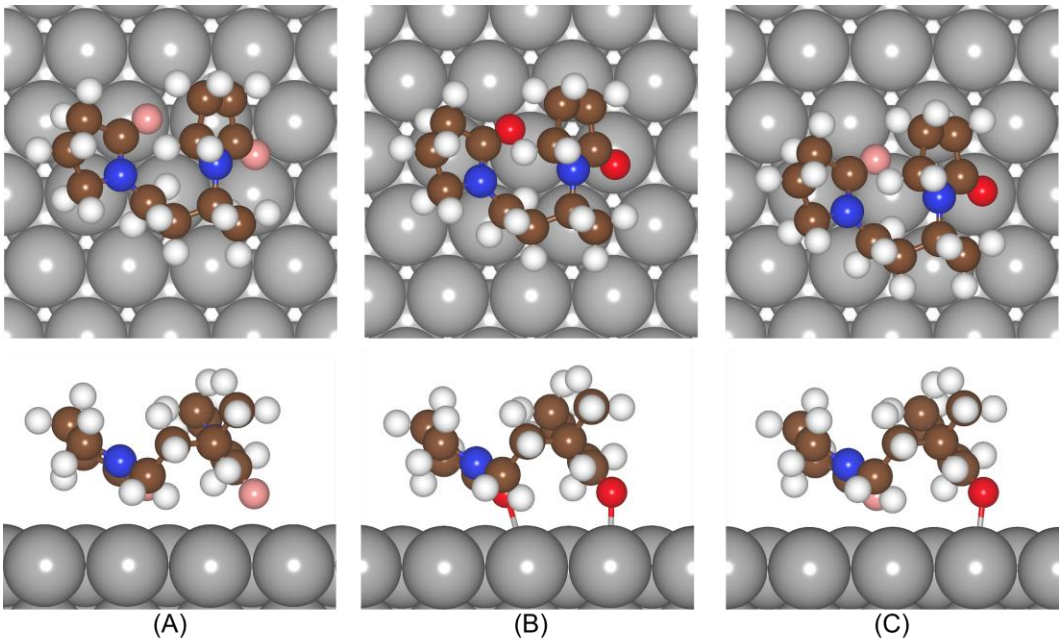

Figure S13. Binding conformations of DVP on Ag(111). Top-down (upper) and side (lower) views of DVP at 0.11 ML coverage on Ag(111) with binding conformation (**A**) 2, (**B**) 3, and (**C**) 4 in **Table S4** (Gray: Ag, Red: bound O, Pink: unbound O, Blue: N, Brown: C, and White: H).

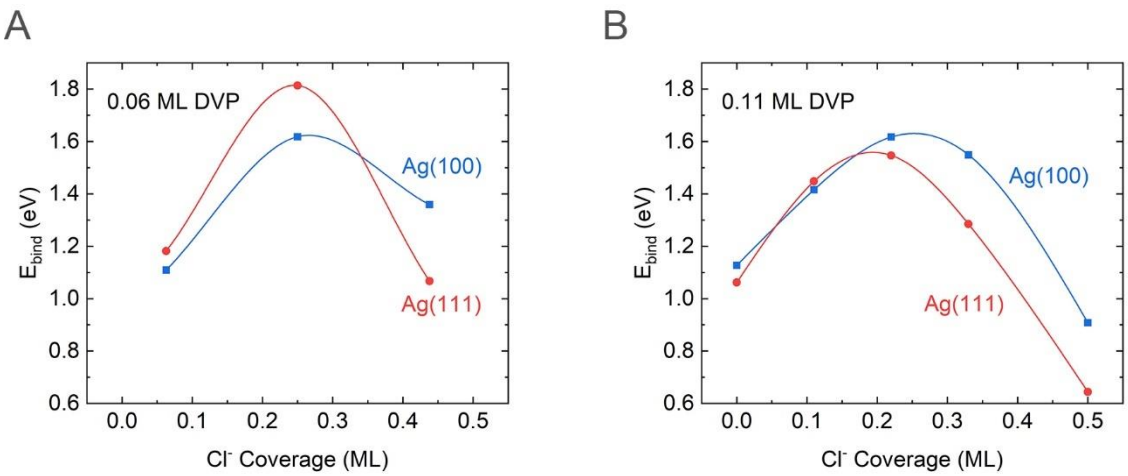

Figure S14. Binding energy of DVP on Ag surfaces as a function of Cl^- surface coverage. (A) 0.06 ML DVP and (B) 0.11 ML DVP.

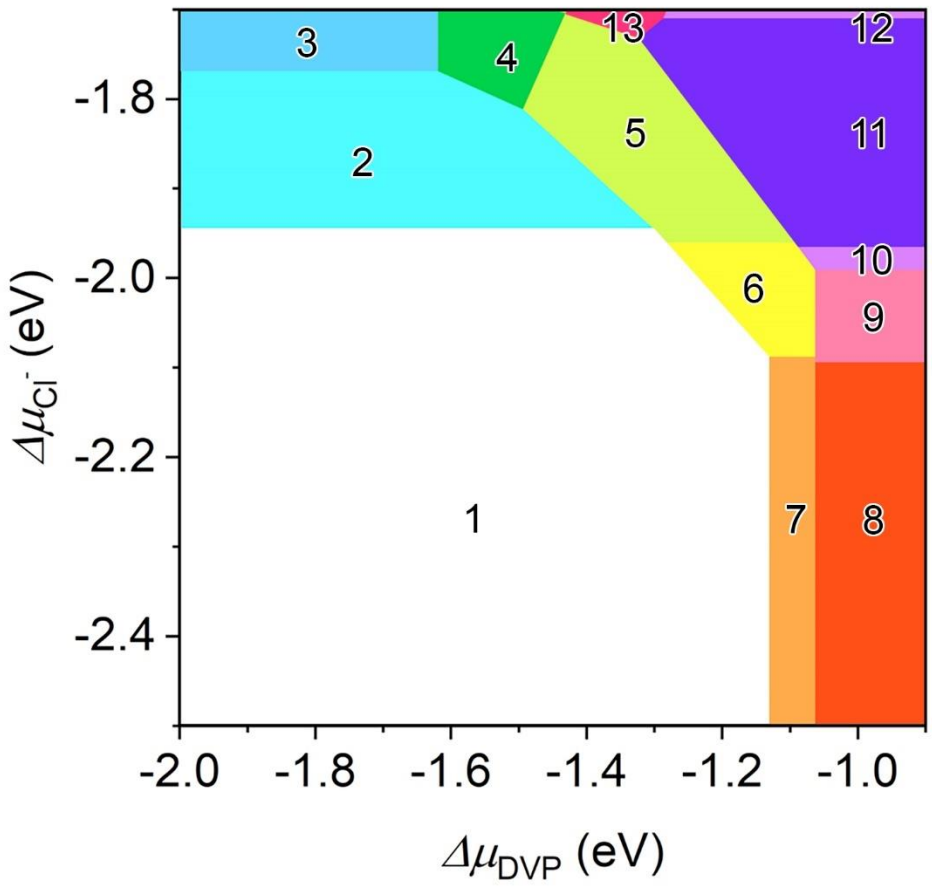

Figure S15. Detailed phase diagram of various regions of Cl and DVP coverage on Ag(100) and Ag(111). The coverage on each surface in each region is shown in **Table S6**.

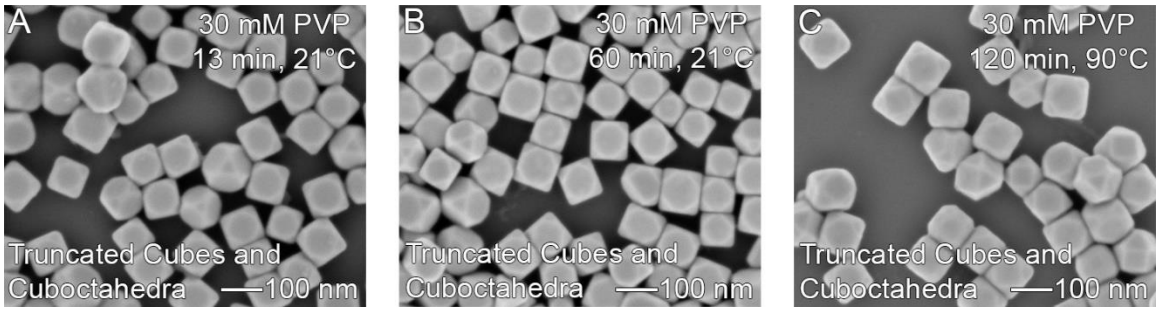

Figure S16. SEM images of the single-crystal seeds after stirring under conditions without silver atom deposition. (A) In 30 mM PVP at 21 °C for 13 minutes. (B) In 30 mM PVP at 21 °C for 60 minutes. (C) In 30 mM PVP at 90 °C for 120 minutes.

References

1. H. Xu and B. J. Wiley, *Chem. Mater.*, 2021, **33**, 8301-8311.
2. N. Murshid, D. Keogh and V. Kitaev, *Part. Part. Syst. Charact.*, 2014, **31**, 178-189.
3. D. M. Zall, D. Fisher and M. Q. Garner, *Analytical Chemistry*, 1956, **28**, 1665-1668.
4. T. Balankura, X. Qi, Y. Zhou and K. A. Fichthorn, *J. Chem. Phys.*, 2016, **145**, 144106.
5. G. Kresse and J. Hafner, *Phys. Rev. B*, 1993, **47**, 558-561.
6. G. Kresse and J. Hafner, *Phys. Rev. B*, 1994, **49**, 14251-14269.
7. G. Kresse and J. Furthmüller, *Phys. Rev. B*, 1996, **54**, 11169-11186.
8. P. E. Blöchl, *Phys. Rev. B*, 1994, **50**, 17953-17979.
9. G. Kresse and D. Joubert, *Phys. Rev. B*, 1999, **59**, 1758-1775.
10. J. P. Perdew, K. Burke and M. Ernzerhof, *Phys. Rev. Lett.*, 1996, **77**, 3865-3868.
11. S. Grimme, *J. Comput. Chem.*, 2004, **25**, 1463-1473.
12. V. G. Ruiz, W. Liu, E. Zojer, M. Scheffler and A. Tkatchenko, *Phys. Rev. Lett.*, 2012, **108**, 146103.
13. Z. Chen and K. A. Fichthorn, *Nanoscale*, 2021, **13**, 18536-18545.
14. Z. Chen and K. A. Fichthorn, *Nanoscale*, 2021, **13**, 13529-13537.